Microchimica Acta (2020) 187:569
https://doi.org/10.1007/s00604-020-04543-w

ORIGINAL PAPER

Rapid and sensitive fluorescence and smartphone dual-mode detection of dopamine based on nitrogen-boron co-doped carbon quantum dots

Sahar Dadkhah[1] · Ali Mehdinia[2] · Ali Jabbari[1] · Ahmad Manbohi[2]

Received: 28 December 2019 / Accepted: 2 September 2020

Abstract

A dual-mode fluorescence and colorimetric biosensor based on nitrogen-boron co-doped carbon quantum dot (N-B CQDs) for rapid and sensitive detection of dopamine (DA) was developed. The quantum dot luminescent materials, N-B CQDs, were prepared by a one-step microwave-assisted method. The N-B CQDs were characterized using SEM, HR-TEM, XRD, FT-IR, Raman, fluorescence, and UV-Vis techniques. The dual-mode assays of fluorescence and colorimetric methods were used for detection of DA. The high fluorescent N-B CQDs mediated turn-off assay for the facile room temperature detection of dopamine via inner filter effect (IFE) and Forster resonance energy transfer (FRET) processes at basic pH. The colorimetric detection of DA was also developed via in-house android application using a smartphone and N-B CQD solution-based nanosensor. The smartphone-based colorimetric biosensors generated more reliable information for quantitative analysis of color changes than the naked eye. Furthermore, a smartphone application with N-B CQD solution-based nanosensor was integrated to monitor the color changes through the DA addition. Wide linear ranges were achieved for DA in the ranges 0.25–50 μM and 5–500 μM with fluorescence and smartphone-based method, respectively. The satisfactory results of the dual-mode detection of DA, not only in aqueous solution, but also in human urine and serum biological sample demonstrated its potential application in biosensing, as a point of care diagnostic tool.

Keywords Dual-mode nanosensor · Quantum dots · Fluorescence detection · Colorimetric detection · Smartphone-based biosensor · Dopamine

Introduction

In recent years, dual-mode sensors have attracted much attention and become an effective strategy in point of care (POC) diagnostic tool, food safety, and environmental monitoring. Compared with single-mode approach, the dual-mode assays such as fluorescence/colorimetry [32, 40], surface-enhanced Raman scattering (SERS)/fluorescence [48], and fluorescence/imaging have been shown to be more sensitive and efficient. Beside the individual advantages of each method used in dual-mode detection, this mode provides a double check readout approach. Therefore, a more reliable and accurate quantitative analysis, especially in biologically complicated sample, can be performed by this approach. To date, some works have been reported about using the dual-mode detection techniques for bio/chemical sensing of some parameters such as pH [40], Cu^{+2} concentration [40, 46], Fe^{+3} concentration [24], glutathione concentration [32], and glucose concentration [29]. Yue et al. have developed a SERS-fluorescence dual-mode pH sensing method using encapsulation of CQDs and 4-mercaptobenzoic acid on the AuNPs as fluorescence and Raman active materials, respectively. They utilized the advantages of both methods such as high specificity of SERS and fast imaging of fluorescence [48]. Park's group has established a dual-mode fluorescence quenching and size reduction hydrogel biosensor for sensitive and selective detection of glucose in human blood. They have incorporated pH-

Electronic supplementary material The online version of this article (https://doi.org/10.1007/s00604-020-04543-w) contains supplementary material, which is available to authorized users.

✉ Ali Mehdinia
mehdinia@inio.ac.ir

[1] Department of Chemistry, Faculty of Science, K. N. Toosi University of Technology, Tehran, Iran

[2] Iranian National Institute for Oceanography and Atmospheric Science, Tehran, Iran

Published online: 15 September 2020

dependent size hydrogel with CQDs in the presence of glucose, which caused simultaneous CQD fluorescence quenching and size reduction [29]. Up to now, among dual-mode detection methods, colorimetric and fluorescent detections have been reported more than the others [24, 40].

Recently, more attentions have been paid to colorimetric biosensors using quantum dots for on-site detection of analytes with naked eye [33]. One of the approaches for visualizing analytes with quantum dots is ratiometric fluorescence technique [6, 30, 46]. For example, Yao's group designed a ratiometric fluorescence nanohybrid probe with two sizes of cadmium telluride QDs with red and green emitting fluorescence for on-site visual determination of copper ions [46]. The second approach is utilizing a hybrid of quantum dot and plasmonic metal nanoparticles, where QDs and metal nanoparticles act as fluorometric and colorimetric reporters, respectively. A dual-mode colorimetric and fluorometric nanosensor based on carbon quantum dots and gold nanoparticles for discriminative detection of glutathione have been developed [32]. Another design of fluorescence/colorimetric sensors consists of triggering the aggregation of the quantum dots in the presence of the analytes. This phenomenon leads to change in photoluminescence properties of quantum dot and subsequently produces color change in the nanosensor [23, 30].

Due to its portability and ubiquitous availability, smartphones have also been emerged as a new generation of analytical tools for biochemical detections. Smartphone has been widely integrated with fluorescence biosensors [47], colorimetric biosensor [49], electrochemical biosensors [28], and microscopic bio imaging [4]. Fluorescent and colorimetric biosensors coupled with smartphone were developed based on image capturing with the digital cameras and image processing algorithm with software application of smartphone. Especially, colorimetric-based assay integrating with smartphone as detector has been much used because of their potential real-time applications in the field of biomedical [34], environmental [38], and food safety [21].

Numerous attempts have been made to synthesize doped fluorescent carbon dots (DFCDs) with various heteroatoms as advanced fluorescent materials. The chemical doping of fluorescent carbon dots is known as a new and effective way to tune the intrinsic properties of CQDs. The photoluminescence properties of QDs could also be adjusted by either doping with a single heteroatom, such as B [37, 52], N [14, 15, 56], S, F, or Cl or co-doping with two or more ones [3, 8, 9, 18, 24]. To date, various doping strategies including hydrothermal (solvothermal), electrochemical treatment, pyrolysis, and microwave-assisted methods have been developed [20, 50]. Compared with the aforementioned strategies for synthesis of DFCDs, microwave-assisted methods are more efficient than the common methods [8]. The fast and green approach using microwave-assisted method has been widely applied to prepare DFCDs with heteroatoms. Microwave-assisted methods not only provide one-pot synthesis route to prepare DFCDs, but also greatly increase the reaction efficiency of elemental doping [8, 56].

In this work, the model target analyte was dopamine (3, 4-dihydroxyphenyl ethylamine, DA), one of the crucial catecholamine neurotransmitters, which play key role in function of central nerve systems [43, 55]. Abnormal levels of DA in the blood cause several disorders, such as schizophrenia, anorexia [40], Ekbom's restless syndrome [57], and Parkinson and Huntington's diseases [55]. As a result, DA can act as an important biomarker for diagnostics of special neurological disorders [43]. Therefore, developing of an accurate and sensitive method for the direct detection of DA at low concentration in complex matrices is highly demanded.

In the present study, a dual-mode fluorescence and colorimetric biosensor for DA was developed by incorporating a smartphone app with solution-based nanosensor. The N-B co-doped CQD solution-based nanosensor exhibited dual response via both fluorescence and visible colorimetric observation for the detection of DA. The N-B CQD solution-based user-friendly and portable nanosensor was also developed by employing an in-house android smartphone app. In the introduced RGB-based (red, green, and blue color space) software, simultaneous analysis was performed by the android app while the image is captured by the camera and the results are displayed on the smartphone.

Experimental

Materials

All chemicals used were of analytical grade chemical reagent. Ultrapure water (Millipore, ≥ 0.05 μS cm^{-1}) was used to prepare solutions in all experiments. Dopamine hydrochloride (DA), ascorbic acid (AA), boric acid, urea, and sodium hydroxide were obtained from Merck (Darmstadt, Germany) and citric acid (CA), disodium hydrogen phosphate, glucose (Glu), and histidine (His) were supplied from Sigma-Aldrich.

Instruments

All fluorescence spectra were recorded from 370 to 800 nm by a fluorescence spectrophotometer (LS-55, Perkin Elmer) using 1-cm path length quartz cuvette and slit widths of 5 and 5 nm for emission and excitation, respectively. UV-Vis absorption measurements were carried out by a UV-Vis spectrophotometer (Perkin Elmer Lambda 25 UV-Vis). The Raman and FT-IR spectra were acquired from 400 to 4000 cm^{-1} using a Fourier transform infrared spectrometer (FT-IR, Bruker TENSOR 27) and Raman spectrometer (μ-Raman Avantes) with a laser of 532 nm (CW mode and

average output power of 100 mW), respectively. Surface microscopic imaging and crystallite size distribution studies were performed using a SEM (ZEISS SIGMA VP FE-SEM with Oxford EDS and Mapping) and high-resolution TEM (FEI Tecnai F20 HR-TEM) microscope. The crystalline structure of N-B CQDs was characterized using an X-ray diffractometer (Panalytical X' Pert Pro) (XRD) by Cu-Kα radiation source.

Microwave-assisted synthesis of luminescent N-B CQDs

The luminescent materials, N-B Co-doped quantum dots, were prepared by some modification of microwave method developed by Bourlinos et al. (2015). Briefly, citric acid monohydrate (0.84 g), urea (0.72 g), and boric acid (0.98 g) were dissolved into 5 mL distilled water and stirred to form a clear solution. Then, the solution was reacted under microwave radiation system with low power (80 W) and moderate temperature (160 °C) for 10 min. After completion of the reaction, the color of the solution changed to green which indicates formation of N-B CQDs. Then, the pH of the final solution was adjusted to neutral and the resulting N-B CQD solution was stored at 4 °C for further use.

Development of in-house android smartphone app

The images were taken with a 20.7-megapixel camera of Sony Xperia. An on-site image processing android-based app that uses an algorithm similar to ImageJ software (U.S. National Institutes of Health, Bethesda, MD, USA) was used for quantifying color intensity and relating it to dopamine concentration. Images were processed in the 8-bit color scale (values ranging from 0 to 255 in which white corresponds to a color intensity of 255 and black corresponds to 0).

The overall work of the app was described in supporting information (Fig. S1). The images were divided into RGB channels in which the maximum of the color intensity was observed on the red channel (R) image. Therefore, the red pixel intensities were used as the signal of the analyte, and these values were used to obtain the calibration curve of dopamine. The image should be taken without a flash with the device positioned as close as possible to the sample container (about 6 cm away).

Detection of dopamine with dual-mode biosensor

Fluorescence spectra of N-B CQDs-based sensor for the detection of DA were recorded by a fluorescence spectrophotometer at room temperature. In a typical experiment, 200 μL of N-B CQDs stock solution (200 μg mL^{-1}) was added to 3600 μL of disodium hydrogen phosphate buffer solution (PB, 10 mM, pH 11). After that, 200 μL of DA solution with different concentrations was added to the above mixture solution. Then, the solution equilibrated for 20 min at room temperature before fluorescence measurement. The fluorescence measurements were carried out by using an excitation wavelength at 366 nm.

The integration of N-B CQD solution-based nanosensor with in-house developed android app using a smartphone provided an effective on-site quantification of DA. In order to quantify colorimetric detection of DA, 2-mL N-B CQDs stock solution (200 μg mL^{-1}), 1.8 mL disodium hydrogen phosphate buffer solution (PB, 10 mM, pH 11), and 200-μL different concentrations of DA standard or sample solution were successively added to a 5-mL tube. Then, the color change of N-B CQD solution-based nanosensor upon reaction with DA was scanned using the smartphone camera through RGB app profiling. All the analysis results were an average of three repetitive measurements ($n = 3$).

Real sample preparation

In order to evaluate the performance of the N-B CQD biosensor in real media, human serums and human urine samples were obtained from healthy volunteers. As proven, the biological matrix exhibits significant blue auto-fluorescence background [7]. For this reason, human serum and urine samples were diluted 50-fold and 10-fold with ultrapure water before analyses, respectively. Then, the fluorescence spectra and color intensity of the samples were recorded under the same procedure mentioned in "Detection of dopamine with dual-mode biosensor".

Results and discussion

Characterization of N-B CQDs

The morphology and size distribution of the N-B CQDs were characterized by FE-SEM and HR-TEM. As shown in the Fig. 1a, the prepared N-B CQDs were all spherical in shape and fairly uniform in size. The HR-TEM images indicate that the final product was N-B CQDs with diameter smaller than 10 nm (Fig. 1b). The colloidal size of N-B CQDs was investigated by the DLS analysis (Fig. S2). The results show that the CQD size distribution was between 70 and 95 nm, which may be due to the agglomeration of the particles [17].

The XRD pattern of the N-B was obtained to characterize the structure of the prepared N-B CQDs. As shown in the Fig. 1c, the diffraction peak centered at $2\theta = 23.2°$ is attributed to the diffraction of the (002) lattice plane. The d-spacing of N-B CQDs ($d = 0.3829$ nm) is larger than that of graphite ($d = 0.334$ nm). As the result was highly consistent with that reported in the literatures [12, 14, 56], enlarging the basal plane

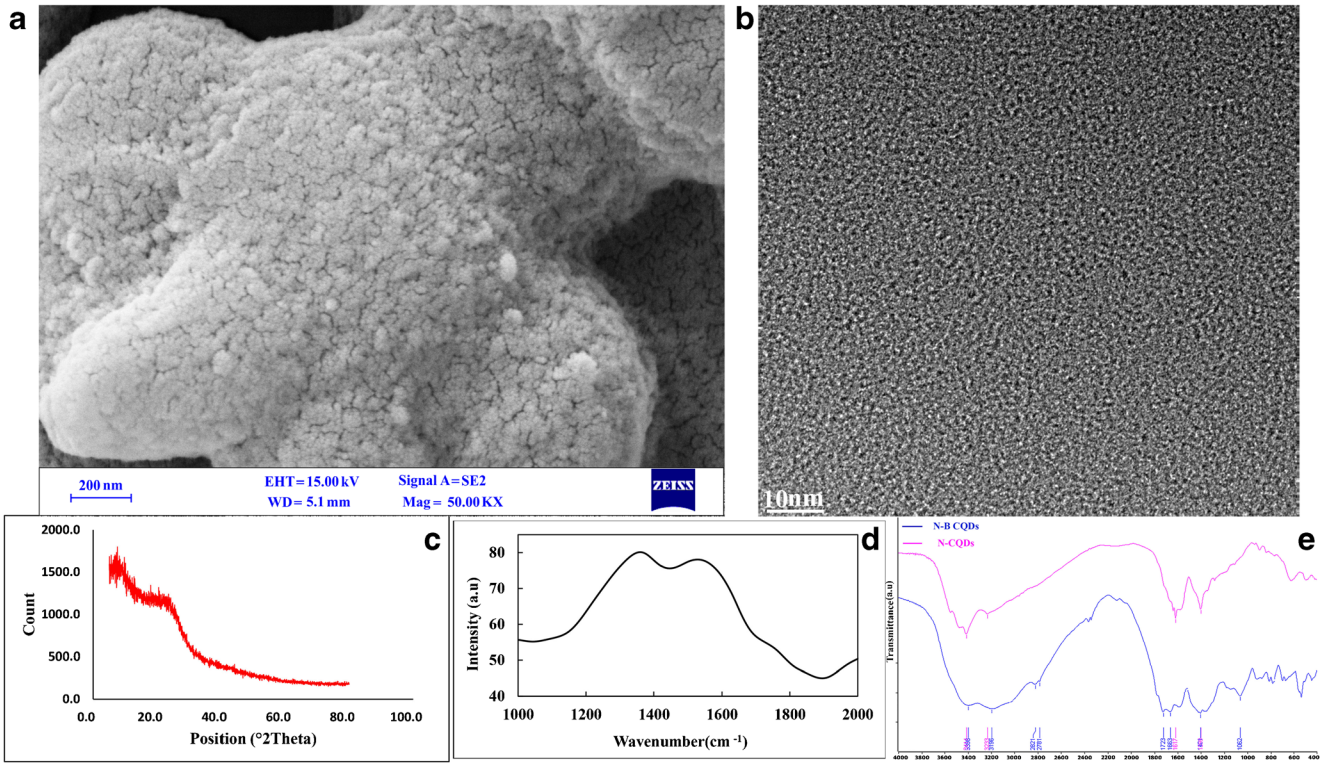

Fig. 1 **a** FE-SEM, **b** HR-TEM images of the synthesized N-B CQDs. **c** XRD, **d** Raman spectra of N-B CQDs. **e** FT-IR spectrum of the N-CQDs and N-BCQDs

spacing of N-B CQDs can be related to the presence of functional group and nitrogen and boron elemental doping.

The Raman spectrum of the N-B CQDs is shown in Fig. 1d. It shows two bands at about 1366 and 1542 cm^{-1}, which are related to the D band (sp3-hybridized) and G band (sp2-hybridized), respectively. The vibrations of carbon atoms in the termination plane of disordered graphite display the D band, that confirms creation of defect sites on the graphitic structures [10, 19, 52]. The results obtained from Raman spectra are in accordance with other characterization and clearly confirm that carbon quantum dots are successfully doped by N-B heteroatom.

Another evidence was provided by comparing FT-IR spectra of N-CQDs and N-B CQDs in Fig. 1e, which displayed an additional absorption peaks located at 1062 cm^{-1} which is assigned to B–C stretching and further confirmed that the B-doping process was effective [3, 37]. The successful doping of nitrogen atoms into the carbon-based quantum dots can be demonstrated by the stretching vibrations of C–N at 1399 cm^{-1}. The broad absorption bands at 3100–3400 cm^{-1} were observed in both spectra of N-CQDs and N-B CQDs, corresponding to the O–H and N–H groups. Moreover, the vibrational absorption band of C=C at 1617 cm^{-1} and C=O at 1723 cm^{-1} was observed [51].

Optical properties of N-B CQDs

The optical properties of the N-B CQDs were investigated by the UV-Vis absorption and the fluorescent spectroscopy. The UV-Vis spectrum of N-B CQDs in an aqueous solution exhibited three absorption peaks at about 250 nm, 340 nm, and 600 nm (Fig. 2a). Generally, the UV-Vis absorption peak in the range of 200–269 nm can be attributed to π–π^* electron transition of the sp^2 C=C band, while the peaks in the range of 270–390 nm are mostly due to transitions of the n–π^* electron transition of the C=O band [14, 44]. A broad peak at about 600 nm is corresponding to the π–π^* of CHN bonding. This absorption peak indirectly explains N-doping of carbon quantum dot [16, 39].

The excitation-dependent fluorescence emission features of the N-B CQDs were further studied by fluorescence spectroscopy. As shown in the Fig. 2b, the maximum emission wavelength is fixed at 445 nm while the excitation wavelength varied from 326 to 406 nm. The strongest blue emission intensity was obtained when the excitation wavelength was fixed at 366 nm. Thus, 366 nm was chosen as the optimal excitation wavelength for the subsequent fluorescence experiment. The results show excitation-independent PL feature of N-B CQDs,

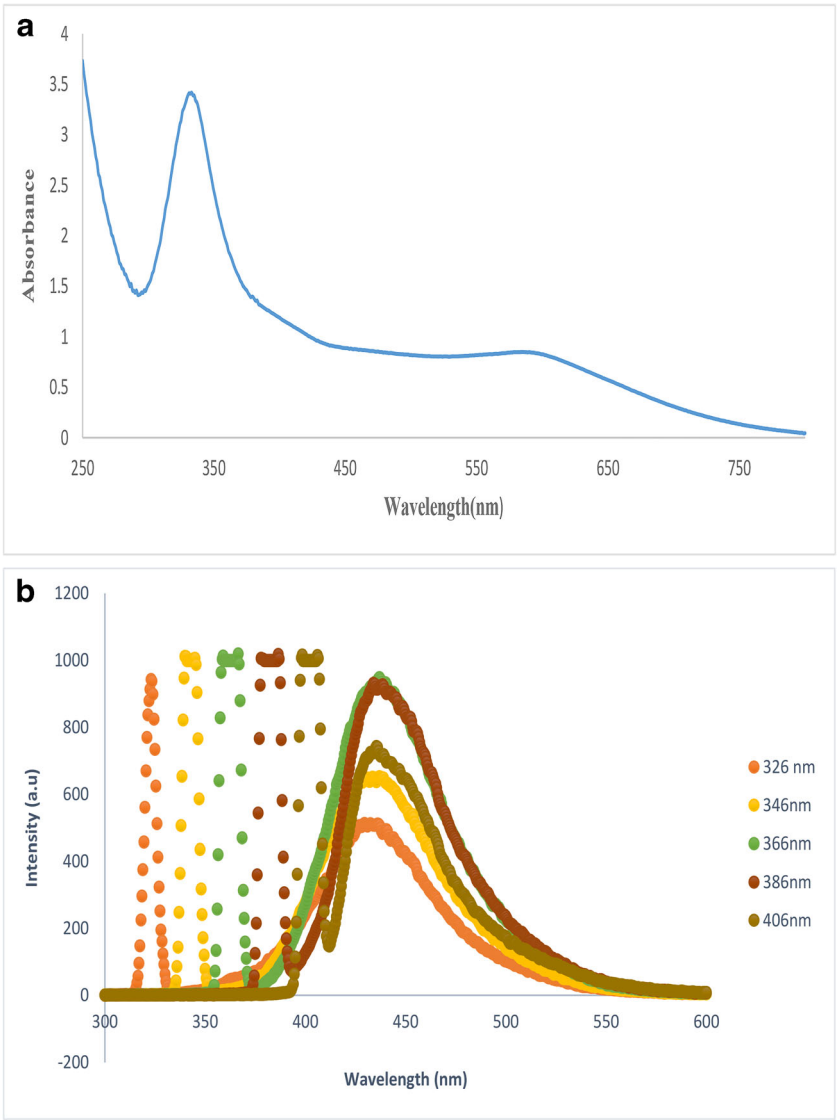

Fig. 2 **a** The UV–Vis absorption and **b** emission spectra of N-B CQDs with different excitation wavelength (326 to 406 nm)

which is usually related to the uniform surface state and size distribution of prepared N-B CQDs [10].

Sensing mechanism investigation

The mechanism of the dual-mode fluorescence and colorimetric N-B CQD nanosensor is based on the fluorescence quenching and color change for the detection of DA.

The possible quenching mechanism of the N-B CQDs/DA system can be explained by this fact that DA can be easily oxidized to DA-quinone under the basic condition and ambient O_2 [1, 2, 5]. Here, the generation of DA-quinone was also investigated by recording the UV-Vis absorption spectra of DA and DA-quinone in water and in the basic condition (pH = 11), respectively (Fig. S3). As illustrated in Fig. S3, the absorption spectrum of produced DA-quinone exhibits effective overlap with the emission peak of N-B CQDs at 445 nm. The primary requirements for both FRET and IFE are overlapping emission spectrum of the fluorophore (N-B CQDs) with the absorption spectrum of the quencher (DA). Besides, the secondary condition for the occurrence of FRET requires the optimum distance between the fluorophore (N-B CQDs) and the quencher (DA). This is only possible if there is some appropriate interaction present between them. Investigation on the surface properties of N-B CQDs by the FT-IR revealed the existence of hydroxyl, carboxyl, and amine group of N-B CQDs, suggesting the possible electrostatic interaction and hydrogen bonding between the N-B CQDs and DA-quinone [27]. Hence, Forster resonance energy transfer (FRET) process could be considered as possible quenching mechanism of N-B CQDs for the detection of DA [54].

To elucidate the exact quenching process of the fluorescence of N-B CQDs by DA, a certain set of experiments was also performed. Thus, to investigate the role of the IFE in the suppression of the fluorescence of N-B CQDs, the

observed fluorescence intensity was corrected by using the Eq. (1). This is applicable for correcting the fluorescence IFE in a spectrum taken via a fluorescence cuvette of 1 cm × 1 cm dimensions [35].

$$\frac{I\ \mathrm{corr}}{I\ \mathrm{obs}} = 10^{\left(A_{(\mathrm{ex})} + A_{(\mathrm{em})}\right)/2}$$

I_{corr}/I_{obs}	correction factor of the fluorescence IFE
I_{corr}	corrected fluorescence intensity
I_{obs}	Observed fluorescence intensity
$A_{(ex)}$	absorbance at the excitation wavelength
$A_{(em)}$	absorbance at the emission wavelength

where A_{em} and A_{ex} are the absorbance at the emission wavelength (445 nm) and the excitation wavelength (366 nm), respectively. I_{obs} is the observed fluorescence intensity and I_{corr} is the corrected fluorescence intensity that is shown in Fig. S9A.

The observed ($\%E_{obs}$) and corrected ($\%E_{corr}$) fluorescence quenching efficiencies and correction factor of the fluorescence IFE at different concentrations of DA are calculated and listed in Table S3. As shown in the Fig. S9B, about 49% of the total suppressed efficiency (%E) is due to IFE of DA to N-B CQDs, which reveals that the IFE mechanism is also an important factor for the fluorescence quenching of the N-B CQD sensor [22]. On the basis of the above-mentioned experimental results, the combination of IFE and FRET could be considered as possible quenching mechanisms of N-B CQDs/DA system.

Moreover, DA-quinone can adsorb onto the surfaces of N-B CQDs through the electrostatic interaction and hydrogen bonding. Also, the adsorption of DA-quinone on the surface of N-B CQDs might induce the aggregation of quantum dots and resulted in color change of the N-B CQDs nanosensor from green to dark brown. Also, the colloidal size of N-B CQDs was investigated by the DLS analysis (Fig. S2). The results show that the CQD size distribution was between 70 and 95 nm in the absence of DA, while the presence of DA increasing in size occurs (about 130–170 nm), which may be due to the aggregation of N-B CQDs by the produced DA-quinone. These results are in agreement with the above description.

Besides that, to more clarify color change in the N-B CQDs/DA system, UV-Vis absorption spectra of produced DA-quinone and N-BCQDs individually and in the form of mixture of DA and N-BCQDs were recorded and the results illustrated in the Fig. S10.

As shown in the Fig. S10, N-B CQDs exhibited a characteristic peak about 340 nm. Also, there is a characteristic peak about 280 nm in the spectra of DA-quinone. The increase of DA-quinone in the N-B CQD solution resulted in the increase of the absorbance at 340 nm and also appears of the absorbance peak at about 280 nm (Fig. S10, mixture of N-B CQDs and DA-quinone). Therefore, the color change of solution is revealed due to the change in absorption ratio of two wavelengths (A_{280}/A_{340} nm).

Moreover, the spectrum of mixture of DA-quinone and N-B CQDs with the mathematical sum of spectra of individual DA-quinone and N-B CQDs was compared and the results listed in Table S4.

The results (Table S4) indicated that absorbance of mixture of DA-quinone and N-B CQDs at 340 nm is approximately equal to the mathematical sum of spectra of individual DA-quinone and N-B CQDs, which are related to N-B carbon quantum dot characteristic peak.

Optimization of experimental conditions

In order to optimize the sensing conditions of N-B CQDs, the influence of the pH value and incubation time on the detection of DA were investigated. The pH value was optimized by monitoring the initial fluorescence intensity of N-B CQD solution in the absence (as control) and the presence of DA in the pH range of 5–12. As shown in Fig. 3a, the fluorescence intensity of N-B CQDs in the presence of DA addition was almost unchanged from acidic (pH 5) to neutral conditions (pH 7), but gradually decreased in the basic conditions (pH 11) due to DA quenching process. The possible reason of fluorescence quenching of N-B CQDs nanosensor is resulted from DA-quinone production in basic condition, while DA-quinone could act as an effective electron acceptor [2, 5].

Furthermore, it can be noted that the changing pH value from acidic to moderate basic condition (pH 11) had little effect on the initial fluorescence intensity (F_0) of N-B CQDs (as control), but the stability and fluorescence intensity of N-B CQDs are detrimentally affected at pH value more than 11.

As results, the highest quenching efficiency for DA and the lowest fluorescence intensity instability for N-B CQDs were detected at pH 11. Therefore, pH 11 was utilized for subsequent sensing strategy of DA using this N-B CQD solution nanosensor. These results are in agreement with the literatures [5, 53].

To enhance the sensitivity and reproducibility of the fluorescence responses of N-B CQD sensor, the effect of incubation time on the fluorescence intensities before and after the addition of DA into N-B CQDs solution was studied. As shown in Fig. 3b, the F_0/F, as function of incubation time, was plotted where the F_0/F represents the fluorescence intensity ratio of N-B CQDs in the absence and presence of DA after same time intervals. As depicted in Fig. 3b, the F_0/F fluorescence ratio increased instantaneously upon addition of DA and reached a maximum in about 25 min. Therefore, 25 min was used for further experiments as incubation time.

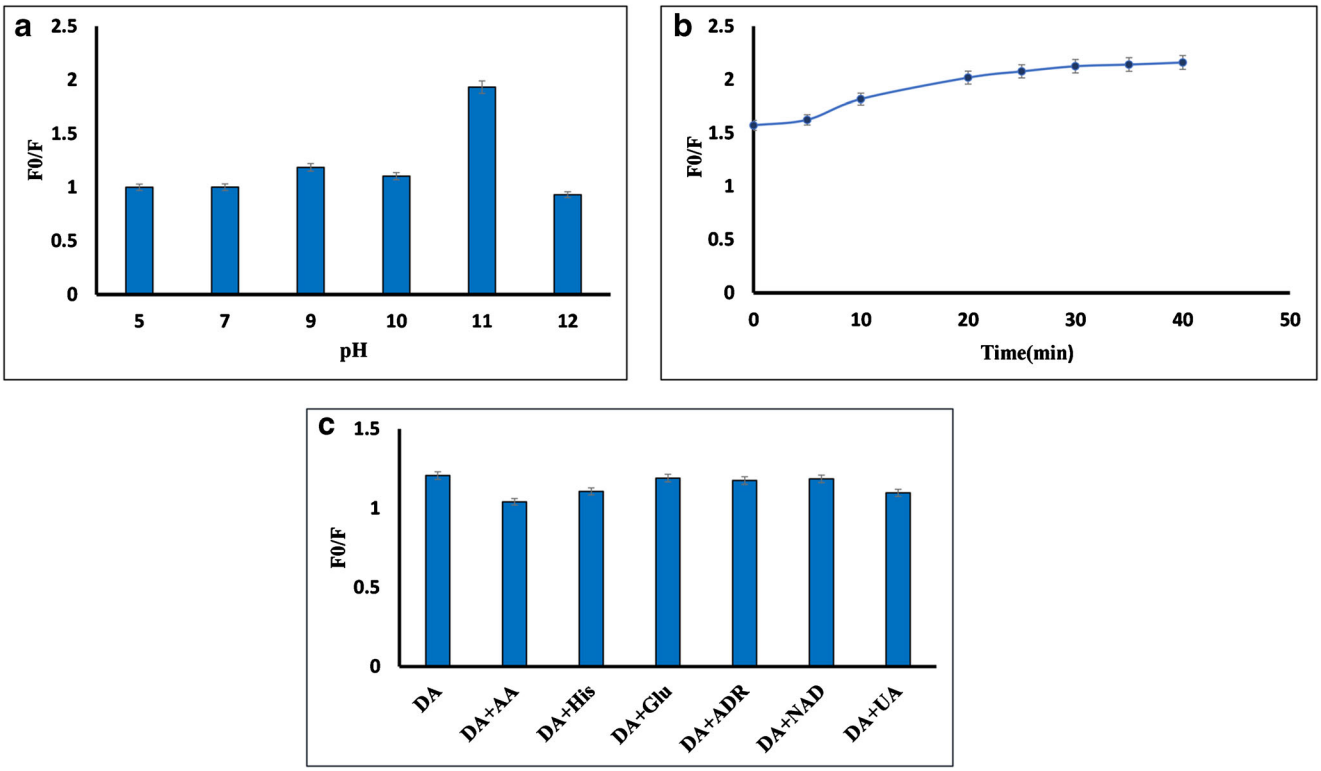

Fig. 3 Optimization investigation of the as-prepared sensing system for DA detection. **a** Effects of the pH value on the fluorescence intensity ratio (F_0/F) of N-B CQD nanosensor in the pH range between 5 and 12. **b** Effects of the incubation time on the fluorescence intensity ratio (F_0/F) of N-B CQD nanosensor in the range between 0 and 40 min. Selectivity studies. **c** The fluorescence intensity ratio (F_0/F) of N-B CQD nanosensor in the presence of DA (10 μM) and other molecules such as histidine amino acid (His, 100 μM), ascorbic acid (AA, 50 μM), glucose (Glu, 100 μM), adrenaline (ADR, 100 μM), and noradrenaline (NAD, 100 μM) and uric acid (UA, 50 μM)

Selectivity of N-B CQD nanosensor

Various common substances in biological samples may interfere with the accuracy of DA detection. To evaluate the selectivity of N-B CQD nanosensor toward DA detection, interference assays were performed by measuring fluorescence quenching of the probe in the presence of DA (10 μM) and other molecules such as histidine amino acid (His, 100 μM), ascorbic acid (AA,50 μM), uric acid (UA, 50 μM), glucose (Glu, 100 μM), adrenaline (ADR, 100 μM), and noradrenaline (NAD, 100 μM). As shown in Fig. 3c, no serious changes happened in the fluorescence intensity ratio of N-B CQD nanosensor in the presence of other interfere molecules. The recovery results of DA in the presence of AA, His, Glu, ADR, NAD, and UA were 86.44%, 91.85%, 98.67%, 97.47%, 98.25%, and 91.17%. It can be observed that in the presence of AA, the fluorescence of quenched sensor slightly recovered because of the reducing nature of AA. However, the recovery results indicated that the satisfactory selectivity toward DA was obtained in the coexistence of AA even in 5-fold concentration.

Moreover, the effects of potassium, sodium, calcium, magnesium, and ferrous cations as major inorganic ions in the human serum were also investigated. As shown in Fig. S4, the binary mixtures of DA and each of these interfering ions were evaluated and their effects on the fluorescence signal were negligible. These results indicated that these common inorganic ions even at 100-fold higher concentration than DA have no obvious effect on the DA detection.

Therefore, competitive experiment of the DA detection in the presence of interferences clearly demonstrated that the N-B CQD nanosensor has acceptable selectivity toward DA detection, which could be related to the described quenching mechanism of nanosensor on "Sensing mechanism investigation".

Detection of dopamine with dual-mode fluorescence and colorimetric nanosensor

Fluorescence detection of DA based on the N-B CQDs

In order to demonstrate the analytical performance of N-B CQDs as fluorescence probes, standard addition method was performed with water, human serum samples to investigate the reliability of nanosensor for sensitive monitoring of DA in biological samples.

As shown in Fig. 4a and b, under the optimized conditions, a good linear regression equation ($F/F_0 = 0.0134\ C_{DA} +$

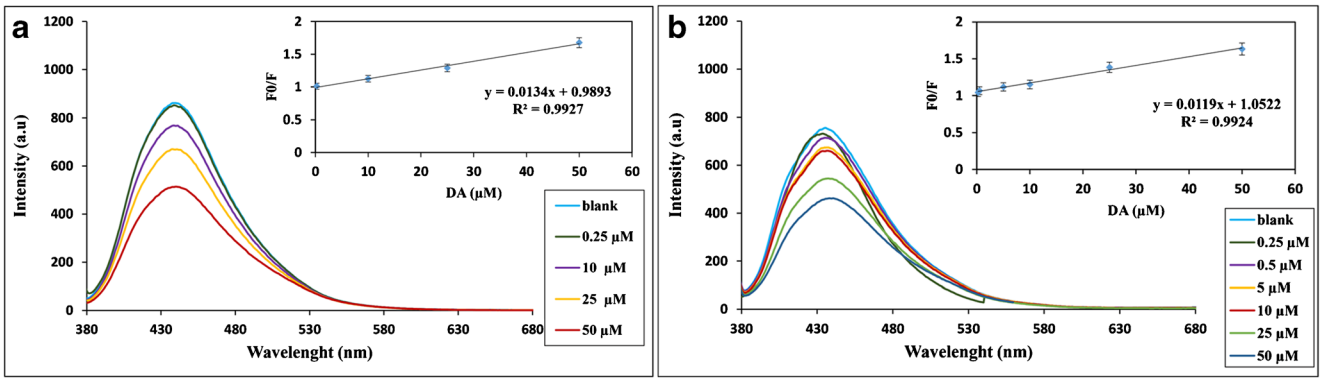

Fig. 4 **a** Fluorescence response of N-B CQDs in the presence of DA with different concentrations. The inset is the calibration curve of DA from 0.25 to 50 μM in the aqueous solution. **b** Fluorescence response of N-B CQDs in the presence of DA with different concentrations. The inset is the calibration curve of DA from 0.25 to 50 μM in the serum sample

0.9893 and $F/F_0 = 0.0119\ C_{DA} + 1.0522$) in the range of 0.25–50 μM with correlation coefficients of 0.9927 and 0.9924 were observed in the aqueous solution and serum samples, respectively. Moreover, based on 3SD/m equation, the limit of detection was determined to be 158 nM where SD and m referred to standard deviation of the blank solution and the slope of the calibration curve of serum, respectively.

To evaluate the practical applications of the N-B CQD nanosensor, a healthy human serum and urine sample, which were spiked with various concentrations of DA, was analyzed. The quantification results of dual-mode detection of DA in the samples are shown in Table 1. The results were also compared with the HPLC method (Fig. S6, Fig. S7, Fig. S8). The recovery values of DA determined by the introduced dual-mode detections are in agreement with HPLC method (Table S1).

To get an idea of the cost-reduction when switching to smartphone-app system from the conventional methods (such as ELISA), approximate costs are provided in Table S2. In comparison with ELISA, the smartphone-based system has the advantage of portability and cost effectiveness. A smartphone and an image processing android-based app are the only required tools. Because of the device simplicity and simple procedure, the cost of the analysis is significantly reduced, aided by the high detection throughput and reduced reagent consumption (€ 4.43 per test). Generally, the price

Table 1 Detection results of DA in healthy human blood serum and urine using the proposed N-B CQDs dual-mode nanosensor ($n = 3$)

Sample	Detection mode	Spiked concentration (μM)	Found (μM) ± SD	Recovery (%)
		0[a]	ND[b]	-
		10	9.43 ± 0.08	94.3
	Fluorescence	20	19.65 ± 0.29	98.25
		50	53.65 ± 0.79	107.3
Serum sample		0 [(a)]	ND	-
	Smartphone	10	10.79 ± 0.13	107.9
		100	96.99 ± 2.54	96.99
		250	259.35 ± 4.61	103.74
		0[c]	ND[b]	-
		0.5	0.48 ± 0.02	96.94
	Fluorescence	1.25	1.21 ± 0.05	96.8
		5	5.15 ± 0.17	103.14
Urine sample		0[c]	ND	-
	Smartphone	10	10.46 ± 0.46	104.6
		25	25.4 ± 1.03	101.6
		50	52.94 ± 2.85	105.88

[a] Healthy human blood serum sample without spike

[b] Not detected

[c] Healthy human urine sample without spike

of the whole system is very low. For more than 20 analyses, the total price of N-B CQD preparation is less than 4.43 EUR. Smart phone detection does not impose a cost on the system, but fluorescence detection system has many lower prices than ELISA or HPLC instrumental methods (Table S2).

Colorimetric detection of DA based on naked eye and smartphone

The color change of N-B CQD probe upon reaction with different concentrations of DA can be observed by naked eyes under natural light without ultraviolet (UV) lamp. In most past reports using quantum dots, evaluations of the color changes in colorimetric methods were normally performed by the naked eye [24, 41, 45, 46]. Thereby, to reduce the risk of personal error and increase the accuracy and reliability of the results, integration of smartphone with colorimetric methods can be effective [31, 49]. As shown in Fig. 5a, the color change of the N-B CQDs probe from green to brown, induced by DA, can be visualized by the naked eye. Then, quantifications of color were measured using the smartphone camera through RGB profiling. The calibration curve was obtained using the R intensity of color change with respect to DA concentration in the linear range of 5–500 μM with correlation coefficient of 0.9914 (Fig. 5b). Moreover, the limit of detection was determined to be a 3.31 μM based on 3SD/m equation (where SD and m referred to standard deviation of the blank solution and the slope of the calibration curve, respectively). Therefore, facile and rapid monitoring of DA can be performed based on in-house developed android app using a smartphone with the introduced N-B CQD nanosensor. Also, the colorimetric detection results of DA using a smartphone are summarized in Table 1.

A comparison of the performance of the introduced dual-mode N-B CQD nanosensor and other sensor based on quantum dots for the detection of DA was performed. As shown in the Table 2, most previously reported nanosensor systems have been focused on fluorescence single readout. While our sensing strategy is based on fluorescence and colorimetric dual-mode detection, our N-BCQD nanosensor provides a limit of detection that is comparable with the reported values observed in most of the sensors based on fluorescence [25, 36,

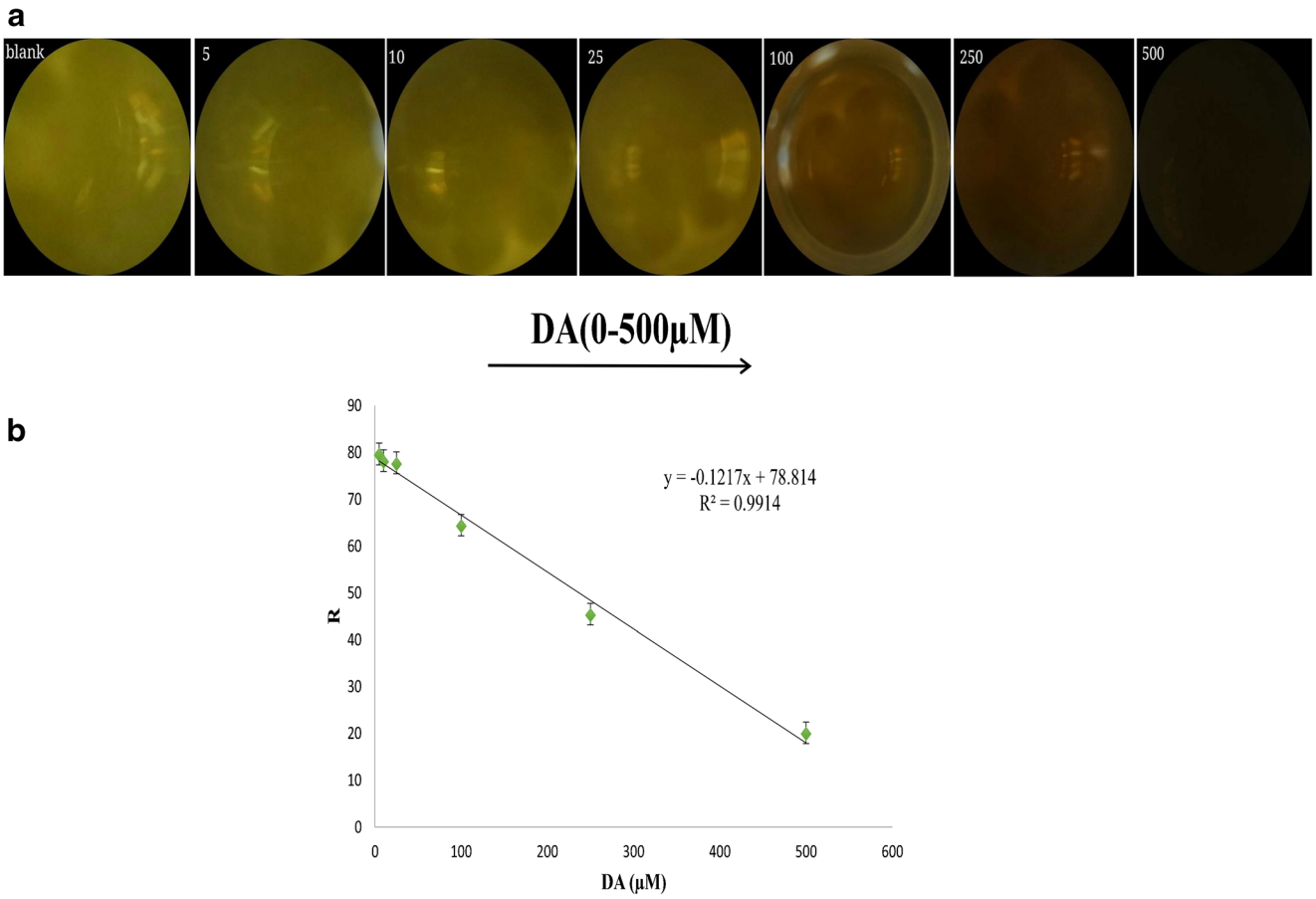

Fig. 5 Smartphone-based colorimetric sensor on N-B CQDs. **a** Images of N-B CQD solution with different concentration of DA, which were directly taken by the smartphone digital camera under natural light. **b** The calibration curve using the R intensity of color change with respect to DA concentration in the linear range of 5–500 μM with excellent linear relationship ($R^2 = 0.9914$)

Table 2 Comparison of different quantum dot-based probes for the detection of DA

Materials	Methods	Experimental conditions	Linear range	Detection limit	Ref
GQDs	Fluorescence	Room temperature and 60 min	0.5–120 μM	0.16 μM	[25]
WS_2 QDs	Fluorescence	60 °C and 90 min	0–50 μM	3.3 μM	[55]
N/B-CDs	Fluorescence	80 min	1.4–260 μM	11 nM	[36]
NB-CQDs	Fluorescence	20 min	0.1–70 μM	0.087 μM	[26]
B-MoS_2 QDs	Fluorescence	1 min	0.25–35 μM		[11]
N-GQDs	Fluorescence and visible paper based test strips	Room temperature and 40 min	1–200 μM	0.07 μM	[5]
CDots-AuNCs	Ratiometric fluorescence	Room temperature and 30 min	5–180 nM	2.9 nM	[13]
Cu-MnxOy/C-dots/TMB composite	Fluorescence and colorimetry (UV)	7 min	0–100 μM 0–75 μM	0.125 μM 0.5 μM	[42]
N-B CQDs	Fluorescence and smartphone detection	Room temperature and 25 min	0.25–50 μM 5–500 μM	0.158 μM 3.312 μM	This work

GQDs graphene quantum dots, *WS_2 QDs* tungsten disulfide quantum dots, *N/B-CDs* boron and nitrogen co-doped carbon dots synthesized from 3-aminophenylboronic acid, *NB-CQDs* nitrogen and boron co-doped carbon quantum dots were synthesized from citric acid, borax, and *p*-phenylenediamine, *B-MoS2 QDs* boronic acid functionalized molybdenum disulfide quantum dots, *N-GQDs* nitrogen-doped graphene quantum dots, *CDots-AuNCs* carbon dots-gold nanocluster hybrid, *Cu-MnxOy/C-dots/TMB composite* Cu-Mn-O microcrystals and C-dots, *TMB* 3,3′,5,5′-tetramethylbenzidine, *N-B CQDs* nitrogen-boron co-doped carbon quantum dot was synthesized from citric acid, boric acid, and urea

55], colorimetric with UV [42], and naked eye in paper-based test strips [5] listed in the Table 1 and Table 2. Though the introduced N-B CQD dual-mode biosensors do not offer higher sensitivity than other methods reported by [11, 13, 26], in the introduced method double check readout provided in short incubation time and moderate condition (room temperature), also good linear range and simple operation come together. Moreover, in our N-BCQD nanosensor, there is no need to other substrates for the colorimetric determination (such as gold nanolaser or TMB). Integrating smartphone with colorimetric detection has reduced some of the limitations of the human eye error in differentiating between color changes and quantitative colorimetric detection of DA easily performed without need of any instruments like UV. To the best of our knowledge, there is no fluorescence and smartphone dual-mode detection strategy being reported for the DA detection until now.

Also, a comparison of the three sensors consists of nitrogen and boron co-doped carbon quantum (Table 2) in terms of synthesis procedure; carbon and dopant sources were also performed.

Tian et al. synthesized N/B CDs through one-pot hydrothermal method (180 °C for 4 h) using 3-aminophenylboronic acid as single source of C, N, and B. In the Liu Yushan et al. paper, nitrogen and boron co-doped carbon quantum dots (NB-CQD) were prepared via one-pot hydrothermal treatment (180 °C for 5 h) of citric acid, borax, and *p*-phenylenediamine as C, B, and N sources, respectively. While in this study, the fast and efficient microwave-assisted method (160 °C for 10 min) was applied to prepare N-B CQDs using citric acid as the carbon source, urea, and boric acid as dopant sources, applying the fast and efficient microwave reaction for synthesis of N-B CQDs can easily reduce the reaction time from 5 h to 10 min, even in lower temperature than hydrothermal methods.

Stability and reproducibility studies

The photostability and the long-term stability of N-B CQDs were investigated. The photostability was monitored by recording fluorescence spectra of N-B CQDs under continuous UV irradiation at different time intervals. As shown in Fig. S5, under UV irradiation during 125 min at 366 nm, a 6.3% decrease in the fluorescence intensity of CQDs was observed. Furthermore, the long-term stability of the N-B CQDs, stored in a refrigerator (4 °C), was checked through fluorescence intensity at the end of 4 weeks. The results indicated that only a 7.2% decreases in the fluorescence intensity of the N-B CQDs were observed.

Moreover, in order to evaluate of inter-day reproducibility of assay, three samples containing DA (20 μM) were measured on three consecutive days by the N-B CQD sensor. The recovery values ranging from 95.2 to 105.3% were obtained, and the relative standard deviation (RSD) was lower than 5.4%. These results revealed that the N-B CQD nanosensor has satisfactory photo stability, long-term stability, and reproducibility for the DA detection.

Conclusion

The fluorescence-based N-B CQD nanosensor was sensitive and specific to low concentration of DA even in common

interfering biomolecule and major cationic ions. The portable developed smartphone system was also promising to become a sensitive tool for quantitative colorimetric measurement and accurate on-site analysis of DA for many applications.

However, the developed N-B CQD dual-mode biosensors may not offer more sensitivity than other sensors in all cases, but double check readout approaches for DA detection can provide advantages of both methods such as selectivity and sensitivity of fluorescence and fast on-site monitoring of colorimetric methods. Integration of smartphone-based colorimetric biosensors with microfluidic paper-based analytical devices (μPADs) as monitoring platform, which are now underway in our lab, are expected to construct more user-friendly and miniaturized platform sensor for many analytes. In the future studies, utilizing the QDs grafted on μPADs, by taking advantages of smartphone application will offer considerable potential in rapid and sensitive point-of-care detections in low-resource settings due to its portability, low cost, and simplicity.

Compliance with ethical standards Informed consent was obtained from all individual participants involved in the study.

Conflict of interest The authors declare that they have no competing of interests.

References

1. Ao H, Qian Z, Zhu Y, Zhao M, Tang C, Huang Y, Feng H, Wang A (2016) A fluorometric biosensor based on functional u/Ag nanoclusters for real-time monitoring of tyrosinase activity. Biosens Bioelectron 86:542–547
2. Ban R, Abdel-Halim E, Zhang J, Zhu J-J (2015) β-Cyclodextrin functionalised gold nanoclusters as luminescence probes for the ultrasensitive detection of dopamine. Analyst 140:1046–1053
3. Bourlinos AB, Trivizas G, Karakassides MA, Baikousi M, Kouloumpis A, Gournis D, Bakandritsos A, Hola K, Kozak O, Zboril R (2015) Green and simple route toward boron doped carbon dots with significantly enhanced non-linear optical properties. Carbon 83:173–179
4. Breslauer DN, Maamari RN, Switz NA, Lam WA, Fletcher DA (2009) Mobile phone based clinical microscopy for global health applications. PLoS One 4:e6320
5. Chen X, Chen S, Ma Q (2017) Fluorescence detection of dopamine based on nitrogen-doped graphene quantum dots and visible paper-based test strips. Anal Methods 9:2246–2251
6. Chen J-Q, Xue S-F, Chen Z-H, Zhang S, Shi G, Zhang M (2018) GelRed/[G3T] 5/Tb3+ hybrid: a novel label-free ratiometric fluorescent probe for H2O2 and oxidase-based visual biosensing. Biosens Bioelectron 100:526–532
7. Diaz-Diestra D, Thapa B, Beltran-Huarac J, Weiner BR, Morell G (2017) L-cysteine capped ZnS: Mn quantum dots for room-temperature detection of dopamine with high sensitivity and selectivity. Biosens Bioelectron 87:693–700
8. Du Y, Guo S (2016) Chemically doped fluorescent carbon and graphene quantum dots for bioimaging, sensor, catalytic and photoelectronic applications. Nanoscale 8:2532–2543
9. Fei H, Ye R, Ye G, Gong Y, Peng Z, Fan X, Samuel EL, Ajayan PM, Tour JM (2014) Boron-and nitrogen-doped graphene quantum dots/graphene hybrid nanoplatelets as efficient electrocatalysts for oxygen reduction. ACS Nano 8:10837–10843
10. Fresco-Cala B, Soriano ML, Sciortino A, Cannas M, Messina F, Cardenas S (2018) One-pot synthesis of graphene quantum dots and simultaneous nanostructured self-assembly via a novel microwave-assisted method: impact on triazine removal and efficiency monitoring. RSC Adv 8:29939–29946
11. Guo X, Huang J, Zeng Q, Wei Y-b, Liu X, Wang L (2019) Boronic acid functionalized molybdenum disulfide quantum dots for ultrasensitive analysis of dopamine basing on synergistic quenched effects from IFE and aggregation. J Mater Chem B
12. Hallaj T, Amjadi M, Song Z, Bagheri R (2018) Strong enhancement of the chemiluminescence of the Cu (II)-H2O2 system on addition of carbon nitride quantum dots, and its application to the detection of H2O2 and glucose. Microchim Acta 185:67
13. He Y-S, Pan C-G, Cao H-X, Yue M-Z, Wang L, Liang G-X (2018) Highly sensitive and selective dual-emission ratiometric fluorescence detection of dopamine based on carbon dots-gold nanoclusters hybrid. Sensors Actuators B Chem 265:371–377
14. Huang H, Li C, Zhu S, Wang H, Chen C, Wang Z, Bai T, Shi Z, Feng S (2014) Histidine-derived nontoxic nitrogen-doped carbon dots for sensing and bioimaging applications. Langmuir 30:13542–13548
15. Karimzadeh A, Hasanzadeh M, Shadjou N, de la Guardia M (2018) Optical bio (sensing) using nitrogen doped graphene quantum dots: recent advances and future challenges. Trends Anal Chem 108:110–121
16. Kim JH, Park JH, Lee JH, Kim JS, Sim M, Shim C, Cho K (2010) Bulk heterojunction solar cells based on preformed polythiophene nanowires via solubility-induced crystallization. J Mater Chem 20(35):7398–7405
17. Kumari A, Kumar A, Sahu SK, Kumar S (2018) Synthesis of green fluorescent carbon quantum dots using waste polyolefins residue for Cu2+ ion sensing and live cell imaging. Sensors Actuators B Chem 254:197–205
18. Kundu S, Yadav RM, Narayanan T, Shelke MV, Vajtai R, Ajayan PM, Pillai VK (2015) Synthesis of N, F and S co-doped graphene quantum dots. Nanoscale 7:11515–11519
19. Li Y, Zhao Y, Cheng H, Hu Y, Shi G, Dai L, Qu L (2011) Nitrogen-doped graphene quantum dots with oxygen-rich functional groups. J Am Chem Soc 134:15–18
20. Li K, Liu W, Ni Y, Li D, Lin D, Su Z, Wei G (2017) Technical synthesis and biomedical applications of graphene quantum dots. J Mater Chem B 5:4811–4826
21. Li X, Yang F, Wong JX, Yu H-Z (2017) Integrated smartphone-app-chip system for on-site parts-per-billion-level colorimetric quantitation of Aflatoxins. Anal Chem 89:8908–8916
22. Li N, Liu SG, Fan YZ, Ju YJ, Xiao N, Luo HQ, Li NB (2018) Adenosine-derived doped carbon dots: from an insight into effect of N/P co-doping on emission to highly sensitive picric acid sensing. Anal Chim Acta 1013:63–70
23. Liang L, Long Y, Zhang H, Wang Q, Huang X, Zhu R, Teng P, Wang X, Zheng H (2013) Visual detection of prion protein based on color complementarity principle. Biosens Bioelectron 50:14–18
24. Liu Y, Duan W, Song W, Liu J, Ren C, Wu J, Liu D, Chen H (2017) Red emission B, N, S-co-doped carbon dots for colorimetric and fluorescent dual mode detection of Fe3+ ions in complex biological fluids and living cells. ACS Appl Mater Interfaces 9:12663–12672
25. Liu H, Li N, Zhang H, Zhang F, Su X (2018) A simple and convenient fluorescent strategy for the highly sensitive detection of

dopamine and ascorbic acid based on graphene quantum dots. Talanta 189:190–195
26. Liu Y, Li W, Wu P, Ma C, Wu X, Xu M, Luo S, Xu Z, Liu S (2019) Hydrothermal synthesis of nitrogen and boron co-doped carbon quantum dots for application in acetone and dopamine sensors and multicolor cellular imaging. Sensors Actuators B Chem 281: 34–43
27. Mao G, Du M, Wang X, Ji X, He Z (2018) Simple construction of ratiometric fluorescent probe for the detection of dopamine and tyrosinase by the naked eye. Analyst 143:5295–5301
28. Nemiroski A, Christodouleas DC, Hennek JW, Kumar AA, Maxwell EJ, Fernández-Abedul MT, Whitesides GM (2014) Universal mobile electrochemical detector designed for use in resource-limited applications. Proc Natl Acad Sci U S A 111: 11984–11989
29. Park H-I, Park S-Y (2018) Smart fluorescent hydrogel glucose biosensing microdroplets with dual-mode fluorescence quenching and size reduction. ACS Appl Mater Interfaces 10:30172–30179
30. Paterson S, De La Rica R (2015) Solution-based nanosensors for in-field detection with the naked eye. Analyst 140:3308–3317
31. Shen L, Hagen JA, Papautsky I (2012) Point-of-care colorimetric detection with a smartphone. Lab Chip 12:4240–4243
32. Shi Y, Pan Y, Zhang H, Zhang Z, Li M-J, Yi C, Yang M (2014) A dual-mode nanosensor based on carbon quantum dots and gold nanoparticles for discriminative detection of glutathione in human plasma. Biosens Bioelectron 56:39–45
33. Song E, Yu M, Wang Y, Hu W, Cheng D, Swihart MT, Song Y (2015) Multi-color quantum dot-based fluorescence immunoassay array for simultaneous visual detection of multiple antibiotic residues in milk. Biosens Bioelectron 72:320–325
34. Sun K, Yang Y, Zhou H, Yin S, Qin W, Yu J, Chiu DT, Yuan Z, Zhang X, Wu C (2018) Ultrabright polymer-dot transducer enabled wireless glucose monitoring via a smartphone. ACS Nano 12: 5176–5184
35. Tanwar AS, Patidar S, Ahirwar S, Dehingia S, Iyer PK (2019) "Receptor free" inner filter effect based universal sensors for nitroexplosive picric acid using two polyfluorene derivatives in the solution and solid states. Analyst 144(2):669–676
36. Tian T, He Y, Ge Y, Song G (2017) One-pot synthesis of boron and nitrogen co-doped carbon dots as the fluorescence probe for dopamine based on the redox reaction between Cr (VI) and dopamine. Sensors Actuators B Chem 240:1265–1271
37. Van Tam T, Kang SG, Babu KF, Oh E-S, Lee SG, Choi WM (2017) Synthesis of B-doped graphene quantum dots as a metal-free electrocatalyst for the oxygen reduction reaction. J Mater Chem A 5:10537–10543
38. Wang L, Li B, Xu F, Shi X, Feng D, Wei D, Li Y, Feng Y, Wang Y, Jia D (2016) High-yield synthesis of strong photoluminescent N-doped carbon nanodots derived from hydrosoluble chitosan for mercury ion sensing via smartphone APP. Biosens Bioelectron 79:1–8
39. Wang H, Sun P, Cong S, Wu J, Gao L, Wang Y et al (2016) Nitrogen-doped carbon dots for "green" quantum dot solar cells. Nanoscale Res Lett 11:27
40. Wang L, Li M, Li W, Han Y, Liu Y, Li Z, Zhang B, Pan D (2018) Rationally designed efficient dual-mode colorimetric/fluorescence sensor based on carbon dots for detection of pH and Cu2+ ions. ACS Sustain Chem Eng 6:12668–12674
41. Wang Y, Yang L, Liu B, Yu S, Jiang C (2018) A colorimetric paper sensor for visual detection of mercury ions constructed with dual-emission carbon dots. New J Chem 42:15671–15677
42. Wang J, Du R, Liu W, Yao L, Ding F, Zou P, Wang Y, Wang X, Zhao Q, Rao H (2019) Colorimetric and fluorometric dual-signal determination of dopamine by the use of Cu-Mn-O microcrystals and C-dots. Sensors Actuators B Chem
43. Weng S, Liang D, Qiu H, Liu Z, Lin Z, Zheng Z, Liu A, Chen W, Lin X (2015) A unique turn-off fluorescent strategy for sensing dopamine based on formed polydopamine (pDA) using graphene quantum dots (GQDs) as fluorescent probe. Sensors Actuators B Chem 221:7–14
44. Xu Y, Wang X, Zhang WL, Lv F, Guo S (2018) Recent progress in two-dimensional inorganic quantum dots. Chem Soc Rev 47:586–625
45. Yan X, Li H, Li Y, Su X (2014) Visual and fluorescent detection of acetamiprid based on the inner filter effect of gold nanoparticles on ratiometric fluorescence quantum dots. Anal Chim Acta 852:189–195
46. Yao J, Zhang K, Zhu H, Ma F, Sun M, Yu H, Sun J, Wang S (2013) Efficient ratiometric fluorescence probe based on dual-emission quantum dots hybrid for on-site determination of copper ions. Anal Chem 85:6461–6468
47. Yu H, Tan Y, Cunningham BT (2014) Smartphone fluorescence spectroscopy. Anal Chem 86:8805–8813
48. Yue S, Sun X, Wang N, Wang Y, Wang Y, Xu Z, Chen M, Wang J (2017) SERS–fluorescence dual-mode pH-sensing method based on Janus microparticles. ACS Appl Mater Interfaces 9:39699–39707
49. Zhang D, Liu Q (2016) Biosensors and bioelectronics on smartphone for portable biochemical detection. Biosens Bioelectron 75:273–284
50. Zhang B-X, Gao H, Li X-L (2014) Synthesis and optical properties of nitrogen and sulfur co-doped graphene quantum dots. New J Chem 38:4615–4621
51. Zhang H, Chen Y, Liang M, Xu L, Qi S, Chen H, Chen X (2014) Solid-phase synthesis of highly fluorescent nitrogen-doped carbon dots for sensitive and selective probing ferric ions in living cells. Anal Chem 86:9846–9852
52. Zhang L, Zhang Z-Y, Liang R-P, Li Y-H, Qiu J-D (2014) Boron-doped graphene quantum dots for selective glucose sensing based on the "abnormal" aggregation-induced photoluminescence enhancement. Anal Chem 86:4423–4430
53. Zhao J, Zhao L, Lan C, Zhao S (2016) Graphene quantum dots as effective probes for label-free fluorescence detection of dopamine. Sensors Actuators B Chem 223:246–251
54. Zhao X, Lei C, Wang Y, Qu F, Zhu S, Wang H, You J (2016) A fluorometric assay for tyrosinase activity and its inhibitor screening based on graphene quantum dots. RSC Adv 6:72670–72675
55. Zhao X, He D, Wang Y, Fu C (2018) Facile fabrication of tungsten disulfide quantum dots (WS2 QDs) as effective probes for fluorescence detection of dopamine (DA). Mater Chem Phys 207:130–134
56. Zheng B, Chen Y, Li P, Wang Z, Cao B, Qi F, Liu J, Qiu Z, Zhang W (2017) Ultrafast ammonia-driven, microwave-assisted synthesis of nitrogen-doped graphene quantum dots and their optical properties. Nanophotonics 6:259–267
57. Zhou X, Wang A, Yu C, Wu S, Shen J (2015) Facile synthesis of molecularly imprinted graphene quantum dots for the determination of dopamine with affinity-adjustable. ACS Appl Mater Interfaces 7: 11741–11747